Effects of the TM/Ce content on the stability of amorphous Al–TM–Ce alloys

2002 J. Phys.: Condens. Matter 14 7949

(http://iopscience.iop.org/0953-8984/14/34/313)

INSTITUTE OF PHYSICS PUBLISHING JOURNAL OF PHYSICS: CONDENSED MATTER

J. Phys.: Condens. Matter **14** (2002) 7949–7954 PII: S0953-8984(02)34937-3

Effects of the TM/Ce content on the stability of amorphous Al–TM–Ce alloys

Zhao Fang, Wu Youshi[1], Shi Yuanchang, Xu Aihua, Zhu Zhiqian and Zhou Guorong

College of Materials Science and Engineering, Shandong University (South Campus), Jinan 250061, Shandong Province, People's Republic of China

E-mail: zhao-fang2001@163.net and wysfmx@jn-public.sd.cninfo.net (Wu Youshi)

Received 15 March 2002, in final form 24 July 2002
Published 15 August 2002
Online at stacks.iop.org/JPhysCM/14/7949

Abstract

X-ray diffraction (XRD) and differential scanning calorimetry were used to investigate the crystallization process of amorphous $Al_{90}TM_xCe_{10-x}$ alloys. Ageing effects were also examined by means of XRD. The structure corresponding to the prepeak for amorphous $Al_{90}Fe_5Ce_5$ alloys is more stable than the amorphous matrix. However, amorphous $Al_{90}Ni_5Ce_5$ alloys are not stable during the first crystallization stage, and even decompose at room temperature. The crystallization onset temperature for amorphous Al–Fe–Ce alloys is much higher than that for amorphous Al–Ni–Ce alloys. This is probably caused by the different stability of the structure corresponding to the prepeak. The crystallization onset temperature increases as the Ce/Ni ratio increases in amorphous $Al_{90}Ni_xCe_{10-x}$ alloys. However, the crystallization onset temperature decreases as the Ce/Fe ratio increases in amorphous $Al_{90}Fe_xCe_{10-x}$ alloys. A better atomic packing results as the Ce content increases due to size mismatch in Al–Ni–Ce systems and as the Fe content increases due to the increasing size of structural units in Al–Fe–Ce systems.

1. Introduction

Aluminium-based alloys produced by rapid solidification have great potential for elevated temperature applications [1]. The amorphous alloys in the Al–TM–RE system with aluminium content up to 90 at.% have been found to have extraordinarily high strength combined with good ductility [2–4]. Furthermore, it has been found that the homogeneous dispersion of fcc Al particles within the amorphous matrix after heat treatment can significantly increase the tensile strength, combining with good bending ductility, as compared with the case for

[1] Author to whom any correspondence should be addressed.

amorphous single-phase alloys with the same composition [5, 6]. The differential scanning calorimetry (DSC) results on the amorphous Al-based alloys usually exhibit two or three crystallization peaks [7, 8]. The first peak, the primary crystallization peak, is caused by the precipitation of Al nanoparticles in the residual amorphous matrix. Usually, the formation of nanocrystals with excellent mechanical properties in Al-based alloys is achieved by overquenching to generate a fully amorphous state and the glass phase is then partially devitrified to produce a nanometre-scale dispersion of Al crystallites in a glassy matrix because the annealing process is easily controllable [9]. In order to tailor the microstructures and the related properties, a clear understanding of the devitrification behaviour of Al-based glasses is needed. The replacement of Ni by Fe increases the thermal stability of the amorphous Al-based alloys, which is often ultimately interpreted on the basis of the fact that Fe has a stronger interaction with Al than Ni. However, the mechanism of the enhancement of the thermal stability of the amorphous alloys is still not clear [10, 11]. Studying of the crystallization process has provided a great deal of knowledge about crystal nucleation and growth, and the thermal stability of the amorphous phase. However, the crystallization behaviour of the present amorphous alloy system is not yet completely understood. In our work, we investigate the crystallization process of amorphous $Al_{90}TM_xCe_{10-x}$ ($x = 3, 5$) alloys with different transition metals (Fe and Ni). The small-angle information from the x-ray diffraction (XRD) pattern during the crystallization process is also investigated.

2. Experiments

Ingots of Al–Ni–Ce and Al–Fe–Ce alloys with the nominal composition were prepared by arc melting a mixture of high-purity Al, Ni (or Fe) and Ce in an argon atmosphere. Amorphous ribbons were prepared by a single-roller melt-spinning technique under a partial argon atmosphere. The diameter of the copper roller was 35 cm, with a typical circumferential velocity of 40 m s^{-1}. The ribbons were $\sim$2 mm in width and $\sim$25 μm in thickness.

The amorphous structure of the ribbon samples was examined by x-ray wide-angle diffraction (XRD) with Cu Kα radiation ($\lambda = 0.1542$ nm) coupled with a graphite monochromator in the diffraction beam. Thermal analysis was performed using a Netzsch DSC-404 system under a pure argon atmosphere. The ageing effects of the amorphous alloys were analysed by means of XRD while they were kept at room temperature for a period of time.

3. Results

The amorphous structures of the $Al_{90}Fe_xCe_{10-x}$ and $Al_{90}Ni_xCe_{10-x}$ ($x = 3, 5$) as-quenched ribbons were examined by XRD. As shown in figures 1(a) and 2(a); the XRD pattern of each contains a main broad peak and a small diffuse peak at small angle. The broad diffuse peaks indicate that the as-quenched ribbons are amorphous. The prepeak is located near $2\theta = 20°$ for the $Al_{90}Ni_5Ce_5$ alloy and around $2\theta = 19.5°$ for the $Al_{90}Fe_5Ce_5$ alloy.

In order to examine the thermal stability and the crystallization process, DSC was performed. Figure 3 shows the DSC curves of amorphous $Al_{90}Ni_3Ce_7$ and $Al_{90}Ni_5Ce_5$ alloys. Figure 4 shows the DSC curves of amorphous $Al_{90}Fe_3Ce_7$ and $Al_{90}Fe_5Ce_5$ alloys. Two or three exothermic peaks are observed in each DSC curve. The first exothermic peak is very weak at low temperatures without a glass transition. The second peak is at high temperatures with a strong exothermic peak. The crystallization onset temperature is about 110 °C for amorphous $Al_{90}Ni_5Ce_5$ and about 165 °C for amorphous $Al_{90}Fe_5Ce_5$. The crystallization

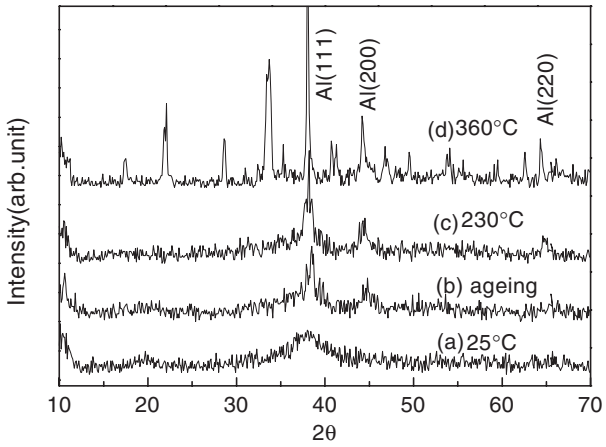

Figure 1. (a), (c), (d) XRD patterns, at different temperatures, of the amorphous $Al_{90}Ni_5Ce_5$ alloys. (b) XRD patterns of the amorphous alloys aged at room temperature for three months.

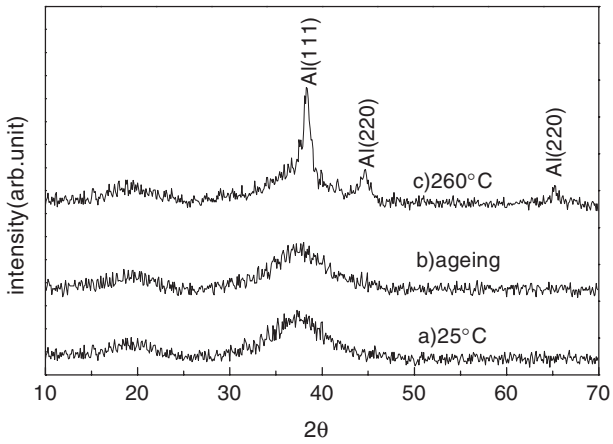

Figure 2. (a), (c) XRD patterns, at different temperatures, of amorphous $Al_{90}Fe_5Ce_5$ alloys. (b) XRD patterns of the amorphous $Al_{90}Fe_5Ce_5$ alloys aged at room temperature for one and a half years.

onset temperature of $Al_{90}Fe_5Ce_5$ is much higher than that of the $Al_{90}Ni_5Ce_5$. It can also be seen that the Ce/TM ratio has a different influence on the crystallization behaviour of these amorphous alloys. From figure 3, the crystallization onset temperature is about 110 and 130 °C for $Al_{90}Ni_5Ce_5$ and $Al_{90}Ni_3Ce_7$ respectively. From figure 4, the crystallization onset temperature is about 165 and 150 °C for $Al_{90}Fe_5Ce_5$ and $Al_{90}Fe_3Ce_7$ respectively. The crystallization onset temperature increases with increasing Ce/Ni ratio in the Al–Ni–Ce system and decreases with increasing Ce/Fe ratio in the Al–Fe–Ce system.

In order to trace the crystallization process, XRD patterns at different temperatures were also examined. XRD patterns, at different temperatures, of $Al_{90}Ni_5Ce_5$ are shown in figures 1(c) and (d). At 230 °C, after the first crystallization peak temperature, the prepeak disappears and fcc Al phase appears. At 360 °C, several intermetallic compounds indicated as Al_3Ni and $Al_{11}Ce_3$ phases are formed. Figure 2(c) shows the XRD pattern of the alloys at 260 °C after the first-crystallization-peak temperature. It can be seen that a fcc Al phase

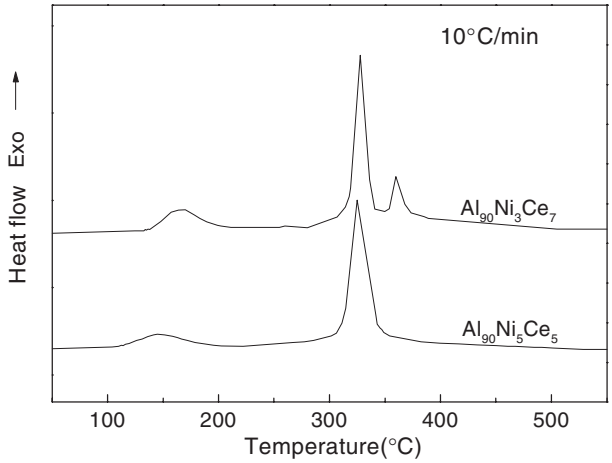

Figure 3. DSC curves of amorphous $Al_{90}Ni_5Ce_5$ alloys.

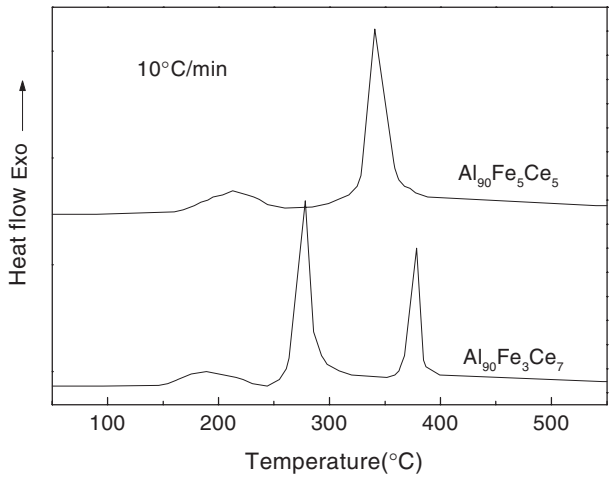

Figure 4. DSC curves of amorphous $Al_{90}Fe_5Ce_5$ alloys.

appears. However, the prepeak still exists in the XRD pattern, which is different from the case for the amorphous $Al_{90}Ni_5Ce_5$ alloys.

The effects of ageing on the amorphous $Al_{90}Ni_5Ce_5$ and $Al_{90}Fe_5Ce_5$ alloys are also investigated. Figure 1(b) shows the XRD patterns of $Al_{90}Ni_5Ce_5$ after ageing at room temperature for three months. It can be seen that fcc Al phase appears and the prepeak becomes more diffuse and weaker. Figure 2(b) shows the XRD patterns of $Al_{90}Fe_5Ce_5$ after ageing at room temperature for one and a half years. It can be seen that the ribbons were still amorphous and the prepeak still exists almost without any change. No evidence of any crystal diffraction peaks appears.

4. Discussion

From figure 2(c), as the fcc Al phase appears during the first crystallization stage for $Al_{90}Fe_5Ce_5$, the prepeak still exists in the XRD pattern, indicating that the structure corresponding to the prepeak is more stable than the amorphous matrix. As shown in figure 1(c), during the first crystallization stage for $Al_{90}Ni_5Ce_5$, a fcc Al phase appears but the prepeak disappears, indicating that the structure corresponding to the prepeak is not stable during the first crystallization stage for this alloy. Therefore, the structure corresponding to the prepeak of amorphous $Al_{90}Fe_5Ce_5$ is more stable than that of $Al_{90}Ni_5Ce_5$. From figures 1(b) and 2(b), the ageing effects also reflect that the stability of the structure corresponding to the prepeak and the amorphous alloys are influenced by the TM elements. It can be seen that after three months' ageing the prepeak becomes diffuse and weak and the fcc Al phase appears for amorphous $Al_{90}Ni_5Ce_5$ alloys. However, the prepeak still exists in the XRD pattern and its intensity does not change very much for $Al_{90}Fe_5Ce_5$ after one and a half years of ageing. This also indicates that the structure corresponding to the prepeak and the amorphous phase of amorphous $Al_{90}Fe_5Ce_5$ alloys is more stable than that of the amorphous $Al_{90}Ni_5Ce_5$ alloys.

As shown in figures 3 and 4, the crystallization onset temperature of amorphous $Al_{90}Fe_5Ce_5$ is much higher than that of amorphous $Al_{90}Ni_5Ce_5$. In these two systems, both Fe and Ni have strong chemical bonding with Al due to sp–d hybridization of Al and TM [12–14]. However, the crystallization onset temperatures of $Al_{90}Fe_5Ce_5$ and $Al_{90}Ni_5Ce_5$ have a large difference, about 55 °C. The enhanced size mismatch can increase the stability of the amorphous matrix by inhibiting Al diffusion [8]. The prepeak shows that structural units with chemical short-range order and medium-range order caused by strong chemical bonds exist in the amorphous alloys [15, 16]. The structural unit size can be estimated according to a formula $R = 2\pi/Q_p$, where Q_p is the prepeak position, and the structural unit is an icosahedral quasi-crystalline structure with Fe as the central atom in Al–Fe–Ce amorphous alloys [15–17]. It has been reported that icosahedral structural units exist in the amorphous $Al_{90}Fe_5Ce_5$ alloys [18]. The structural unit size is about 0.45 nm or so in $Al_{90}Ni_5Ce_5$ and $Al_{90}Fe_5Ce_5$, which is much larger than that for the Al, Fe(Ni) or Ce atoms. As discussed above, the structure corresponding to the prepeak for $Al_{90}Fe_5Ce_5$ is more stable than that of $Al_{90}Ni_5Ce_5$. During the crystallization, the stable structure corresponding to the prepeak can increase the difficulty of the atomic diffusion, consequently preventing fcc Al precipitating from the amorphous matrix. Therefore, the large difference of the crystallization onset temperatures and the relative alloy stability at room temperature are probably caused by the different stabilities of the structures corresponding to the prepeak.

Although both Ni and Fe have the smaller atomic size than Ce and Al–Ni and Al–Fe have nearly have the same bond length, 0.246–0.249 nm [12–14], the Ce/TM ratio has different effects on the crystallization behaviour in amorphous $Al_{90}Fe_xCe_{10-x}$ and $Al_{90}Ni_xCe_{10-x}$ systems. From figure 3, the crystallization onset temperature increases as the Ce content increases for amorphous $Al_{90}Ni_xCe_{10-x}$ alloys. However, the amorphous $Al_{90}Fe_xCe_{10-x}$ alloys behave in exactly the opposite way. As shown in figure 4, the crystallization onset temperature decreases as Ce content increases. The nearest neighbours of TM and RE are Al atoms [12, 13, 19], so enhanced size mismatch can lead to better atomic packing [8]. The structure corresponding to the prepeak is not stable during the crystallization process for Al–Ni–Ce amorphous alloys. During the first step of the crystallization process, the structure corresponding to the prepeak decomposes. A higher Ce versus Al content implies better atomic packing due to the size mismatch during the first step of the crystallization process. This decreases Al diffusivity, which leads to a higher crystallization onset temperature. However, the structure corresponding to the prepeak of amorphous Al–Fe–Ce systems is stable during

the first crystallization stage. The structural unit is much larger than that for the Al, Fe or Ce atoms, and is equal to large atoms which can produce large size effects, leading to better atomic packing due to size mismatch. The higher crystallization onset temperature with increasing Fe content implies that a better atomic packing is produced; this is probably caused by the increasing Fe central structural unit size as Fe content increases.

Acknowledgment

This work was supported by the Natural Science Foundation of Shandong Province (NO Y2000b02).

References

[1] Sun W S, Quan M X and Li S L 1997 *J. Mater. Sci.* **32** 6609
[2] He Y, Poon S J and Shiflet G J 1988 *Science* **241** 1640
[3] Shiflet G J, He Y and Poon S J 1988 *J. Appl. Phys.* **64** 1988
[4] Inoue A, Ohtera K, Tsai A P and Masumoto T 1988 *Japan. J. Appl. Phys.* **27** L280
[5] Kim Y K, Inoue A and Masumoto T 1991 *Mater. Trans. JIM* **32** 331
[6] Kim Y H, Inoue A and Masumoto T 1990 *Mater. Trans. JIM* **31** 747
[7] Dunlap R A, Yewondwossen M H, Srinivas V, Christie I A, McHenry M E and Lloyd D J 1990 *J. Phys.: Condens. Matter* **2** 4315
[8] Saini S, Zaluska A and Altounian Z 1999 *J. Non-Cryst. Solids* **250–252** 714
[9] Kim Y K, Soh J R, Kim D K and Li H M 1998 *J. Non-Cryst. Solids* **242** 122
[10] Inoue A and Masumoto T 1991 *Mater. Sci. Eng.* A **133** 6
[11] Jin H W, Kim Y J and Park C G 2001 *J. Mater. Sci.* **36** 2089
[12] Hsieh H Y, Toby B H, He Y, Poon S J and Shiflet G J 1990 *J. Mater. Res.* **5** 2807
[13] Hsieh H Y, Egami T, He Y and Poon S J 1991 *J. Non-Cryst. Solids* **135** 248
[14] Yamamoto I, Van Zytveld J and Endo H 1996 *J. Non-Cryst. Solids* **205–207** 728
[15] Zhang Lin, Wu Youshi, Bian Xiufang, Li Hui, Wang Weiming, Li Jingguo and Lun Ning 1999 *J. Phys.: Condens. Matter* **11** 7959
[16] Zhang Lin, Wu Youshi, Bian Xiufang, Li Hui, Wang Weiming and Wu Si 2000 *J. Non-Cryst. Solids* **262** 169
[17] Vateva E and Savova E 1995 *J. Non-Cryst. Solids* **192–193** 145
[18] Zhang Chuanjiang and Wu Youshi 2001 *J. Phys.: Condens. Matter* **13** L647
[19] Matsubara E, Waseda Y, Inoue A, Ohtera H and Masumoto T 1989 *Z. Naturf.* **44** 814